*Friction* **11**(4): 635–646 (2023)
https://doi.org/10.1007/s40544-022-0633-6
ISSN 2223-7690
CN 10-1237/TH
RESEARCH ARTICLE

# Rigid–flexible hybrid surfaces for water-repelling and abrasion-resisting

**Songtao HU[1], Weifeng HUANG[2], Jinbang LI[3], Tom REDDYHOFF[4], Xiaobao CAO[5], Xi SHI[1,*], Zhike PENG[1,6], Andrew DEMELLO[5], Daniele DINI[4]**

[1] *State Key Laboratory of Mechanical System and Vibration, Shanghai Jiao Tong University, Shanghai 200240, China*

[2] *State Key Laboratory of Tribology, Tsinghua University, Beijing 100084, China*

[3] *School of Mechanical Engineering and Mechanics, Ningbo University, Ningbo 315211, China*

[4] *Department of Mechanical Engineering, Imperial College London, London SW7 2AZ, UK*

[5] *Department of Chemistry and Applied Biosciences, ETH Zurich, Zurich 8093, Switzerland*

[6] *School of Mechanical Engineering, Ningxia University, Yinchuan 750021, China*

*Received: 29 September 2021 / Revised: 23 November 2021 / Accepted: 08 April 2022*



**Abstract:** Droplets impacting solid superhydrophobic surfaces is appealing not only because of scientific interests but also for technological applications such as water-repelling. Recent studies have designed artificial surfaces in a rigid–flexible hybrid mode to combine asymmetric redistribution and structural oscillation water-repelling principles, resolving strict impacting positioning; however, this is limited by weak mechanical durability. Here we propose a rigid–flexible hybrid surface (RFS) design as a matrix of concave flexible trampolines barred by convex rigid stripes. Such a surface exhibits a 20.1% contact time reduction via the structural oscillation of flexible trampolines, and even to break through the theoretical inertial-capillary limit via the asymmetric redistribution induced by rigid stripes. Moreover, the surface is shown to retain the above water-repelling after 1,000 abrasion cycles against oilstones under a normal load as high as 0.2 N·mm$^{-1}$. This is the first demonstration of RFSs for synchronous waterproof and wearproof, approaching real-world applications of liquid-repelling.

**Keywords:** surface; droplet impact; hydrophobic; abrasion

## 1 Introduction

Impacting behaviors between solid superhydrophobic surfaces (high contact angle and tiny adhesion) and liquid droplets are appealing not only because of their scientific interests but also for technological applications including liquid-repelling [1], anti-icing [2], energy harvesting [3], and directional transport [4]. Such behaviors arise from the interplay of morphological and chemical surface attributes [5], manifesting as good impalement resistance against droplet intrusion and short droplet–solid contact time at impact. Impinging droplets will contact, spread, retract, and bounce off a superhydrophobic surface in circular symmetry, limiting the contact time by balancing the inertia and capillarity [6]. Accordingly, morphological curvatures have been created on rigid surfaces to remarkably reduce the contact time via breaking symmetrical bouncing and redistributing momentum and mass with regard to impinging droplets [7–12]. In contrast with the rigidity-based asymmetric redistribution principle above, flexible design has been proposed to reduce the contact time by weakening the impacting loads via surface oscillations at impact, shifting the related research from statics to dynamics [13–16]. However, the above two water-repelling principles (rigidity-based asymmetric redistribution and flexibility-based structural oscillation) urge a

* Corresponding author: Xi SHI, E-mail: xishi@sjtu.edu.cn

strict alignment between impinging droplets and surface morphological features. Recently, researchers have reported a flexibility-patterned surface (as a matrix of flexible trampolines barred by rigid stripes) to combine these two principles [17]. Such a rigid–flexible hybrid design can cope with the positioning problem because the contact time reduction will be triggered by the asymmetric redistribution or structural oscillation principle when droplets impact the rigid stripes or flexible trampolines, respectively. Herein, as the rigid stripe and flexible trampoline are in the same level, when droplets impact a rigid stripe, the neighboring flexible trampolines will deform downwards to construct a convex curvature together with the rigid stripe.

Besides the good repellency against droplet intrusion mentioned above, robust mechanical durability is another vital issue for designing superhydrophobic surfaces, which mainly includes adhesive and abrasion durability [18]. In comparison to adhesive durability that studies the detachment of waterproof coatings from the substrate, abrasion durability has been more sufficiently investigated since the rubbing of water-repelling surfaces is common in daily applications [19–21]. Among the studies on designing abrasion-resisting waterproof surfaces, a two-level morphology has been popularly adopted [22–26]. In such design, the primary-level and large-scale structure is arranged to sacrifice under abrasion so as to protect the secondary-level and small-scale structure, thus minimizing the alteration of morphological and chemical surface attributes to delay water-repelling failure. The most recent work has reported a convex micro frame containing concave pockets that is house water-repelling but mechanically fragile nanostructures [26]. As the frame acts as mechanical armors, the nanostructures have been protected from material removal, yielding robust abrasion resistance.

Here, we intensify the mechanical durability of rigid–flexible hybrid water-repelling surfaces [17] by coupling the frame-pocket abrasion-resisting design [26]. More precisely, rigid stripes are designed as convex frames but flexible trampolines are designed as concave pockets (Fig. 1(a)). By this, the rigid stripes can trigger asymmetric redistribution principle for water-repelling and is able to undertake normal pressure and horizontal shear for abrasion-resisting; and the flexible trampolines will retain structural oscillation for water-repelling after abrasion due to the protection of the rigid stripes. Using wire cutting and sprayed coating, we realize the design and verify its water-repelling enhancement on reducing contact

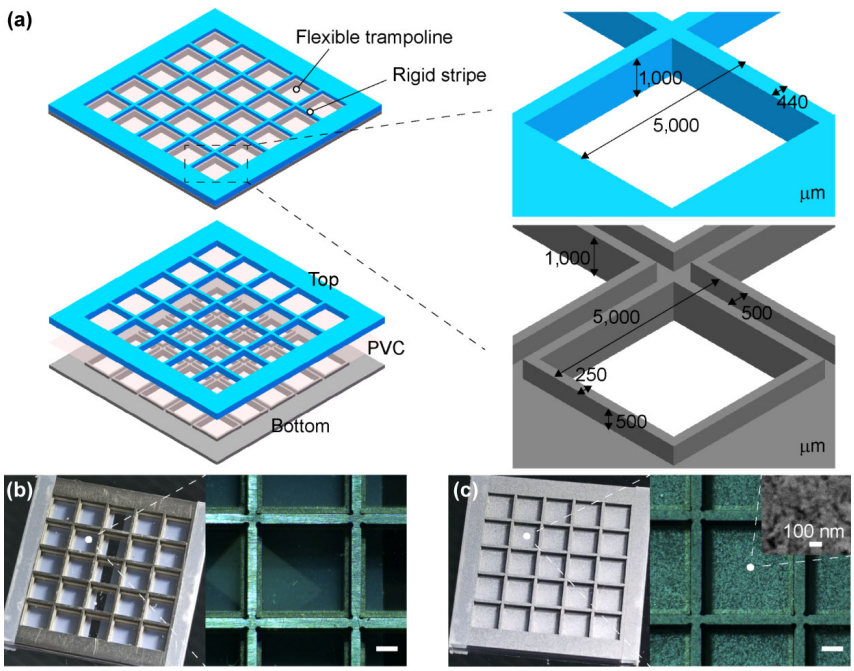


**Fig. 1** RFS. (a) Design of an RFS, as a matrix of concave flexible trampolines barred by convex rigid stripes. (b, c) Images of the RFS fabricated by wire cutting and coated with low-surface-energy chemical particles. Scale bar: 1 mm.

time and mechanical robustness against oilstone abrasion. We believe this study to be the very first demonstration of rigid–flexible hybrid surfaces (RFSs) for synchronous waterproof and wearproof, thereby approaching real-world applications of liquid-repelling.

## 2 Methods

### 2.1 Surface fabrication and characterization

Wire cutting was used to fabricate the top and bottom parts made of steel. A 10-μm commercial thin film made of polyvinyl chloride (PVC) was packaged by the top and bottom parts like a sandwich. Although the top and bottom parts were self-assembled by inserting the top part into the bottom one, tapes were used at the edges to fasten the assembly. Commercial Ultra-Ever Dry (Ultra Tech International Inc., USA) was sprayed to coat low-surface-energy chemical particles [4, 17, 26, 27]. Morphological images of the surfaces were taken with an optical microscope (LW300LMDT, Cewei Guangdian, China).

### 2.2 Compression test

The load–displacement relationship of flexible trampoline was measured on a tensile-pressure tester (ZQ990A, Zhiqu Precision Instruments, China) in pressure mode with a spherical indenter compressing the trampoline center. Referring to a certain displacement for the indenter, the corresponding load between the indenter and the trampoline was recorded. The measurement was repeated three times for repeatability.

### 2.3 Static water repellency test

The contact angle and adhesion of 2-μL deionized water droplets on the surfaces were investigated on a contact angle goniometer (SDC-100, Sindin, China) in sessile drop mode under controlled temperature (25 °C) and relative humidity (45%). For contact angle measurements, the characterization was conducted 30 s after the droplet contacted the surfaces to ensure an equilibrium. The measurement was repeated three times for each surface.

### 2.4 Kinetic water repellency test

An electrically-controlled microsyringe pump was used to generate and release 8-μL deionized water droplets at a specified height with the assistant of a linear motor. Impacting behaviors of water droplets on the surfaces were recorded by a high-speed camera (5KF10, FuHuang AgileDevice, China) at a rate of 5000 fps. The measurement was repeated three times for each surface position at each releasing height.

### 2.5 Abrasion test

Abrasion was conducted by loading and sliding a triangular (85°, 47.5°, and 47.5°) oilstone against the surfaces on a self-built tribological test rig. The surfaces were held as the lower stationary specimen, while the oilstone had a reciprocating motion as the upper specimen controlled by a linear motor. During the abrasion test, the oilstone was declined to approach a line contact with the surfaces at a normal load of 3 N, and was then slid over the surface at a velocity of 1 $mm \cdot s^{-1}$. The horizontal shear was recorded at a step of 0.1 s to calculate the ratio of the horizontal shear to the normal load known as the coefficient of friction.

## 3 Results and discussion

### 3.1 Design and fabrication

We first designed rigid top and bottom parts (Fig. 1(a)). After packaging a flexible thin film by inserting the top part into the bottom part as similar to a sandwich, an RFS can be achieved as a matrix of concave flexible trampolines barred by convex rigid stripes. As per to the design of the top and bottom parts, for the flexible trampolines, the pitch and side lengths were set to 5,000 and 4,560 μm, respectively; and the height (the distance from the PVC film to the nethermost side of the bottom part) was set to 1,000 μm. For the rigid stripes, the width was set to 440 μm; and the height (the distance from the upmost side of the top part to the PVC film) was set to 500 μm. According to previous water-repelling works, contact time reduction is envisioned to be triggered by the asymmetric redistribution principle when a droplet impacts a rigid stripe [7–12, 17], and will be triggered by the structural

oscillation principle when the impact occurs on a flexible trampoline [13–17]. Meanwhile, referring to previous abrasion-resisting works, the convex rigid stripes are able to undertake normal pressure and horizontal shear so as to protect the concave flexible trampolines that are water-repelling but mechanically fragile. To realize our design, wire cutting was used to fabricate the top and bottom parts made of steel, which packaged the PVC film like a sandwich (Fig. 1(b)). Of note, although the top and bottom parts were self-assembled by inserting the top part into the bottom one, tapes were used at the edges to fasten the assembly. Eventually, commercial Ultra-Ever Dry (Ultra Tech International Inc., USA) was sprayed to coat low-surface-energy chemical particles (Fig. 1(c)).

Note that the RFS surface was designed as a matrix consisting of 5 × 5 units as prototype, and would be simple to extend the size for industrial applications. As references, we also designed and fabricated the corresponding rigid surface (RS) and smooth surface (SS) (Fig. 2). Also noteworthy is the nomenclature RFST and RFSS for the trampoline and stripe regions of the RFS, respectively, and RST and RSS for the trampoline and stripe regions of the RS, respectively.

### 3.2 Static water repellency

We investigated the mechanics of flexible trampolines on the RFS by experimentally capturing the load–displacement relationship (Fig. 3(a)). As the height of flexible trampolines was designed as 1,000 μm, the displacement was changed from 0 to 900 μm, providing the corresponding load with an exponential slope that violates Hooke's law. The measurement was repeated three times for uncoated and coated conditions, showing good repeatability. Under the same displacement, the load for the coated RFS was higher than that for the uncoated RFS, indicating a higher stiffness due to the presence of low-surface-energy chemical particles.

To investigate static water repellency, the fabricated surfaces (RFS, RS, and SS) were controlled to contact and slide over hanging water droplets on a contact angle goniometer. When the SS started to contact the droplet (Fig. 3(d)), the droplet beaded up on the surface; even if the SS continued to lift up to further compress the droplet, the droplet preferred to climb up along the microsyringe needle rather than wetting the surface; and the droplet was eventually trapped by the needle. All these indicate great static water repellency for the SS, which is ascribed to the low-surface-energy chemical modification. Also, the SS was easy to slide over the droplet, again highlighting the great static water repellency. The same phenomena can be observed when the trampolines and stripes of the RFS and RS contacted and slid over hanging droplets (Figs. 3(b) and 3(c)), confirming the great repellency in response to static water droplets. Note that no structural deformation was observed on the

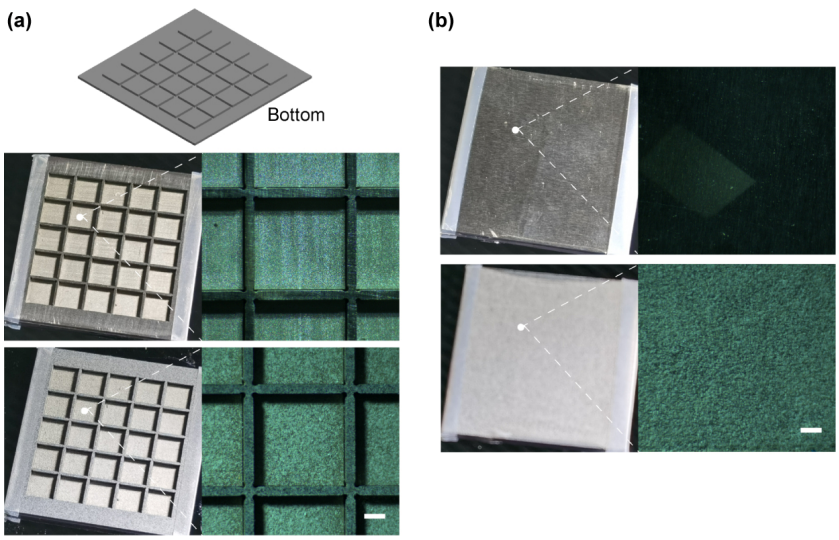


**Fig. 2** Reference surfaces. (a) Images of an RS as a matrix of rigid trampolines barred by rigid stripes. (b) Images of an SS. Scale bar: 1 mm.

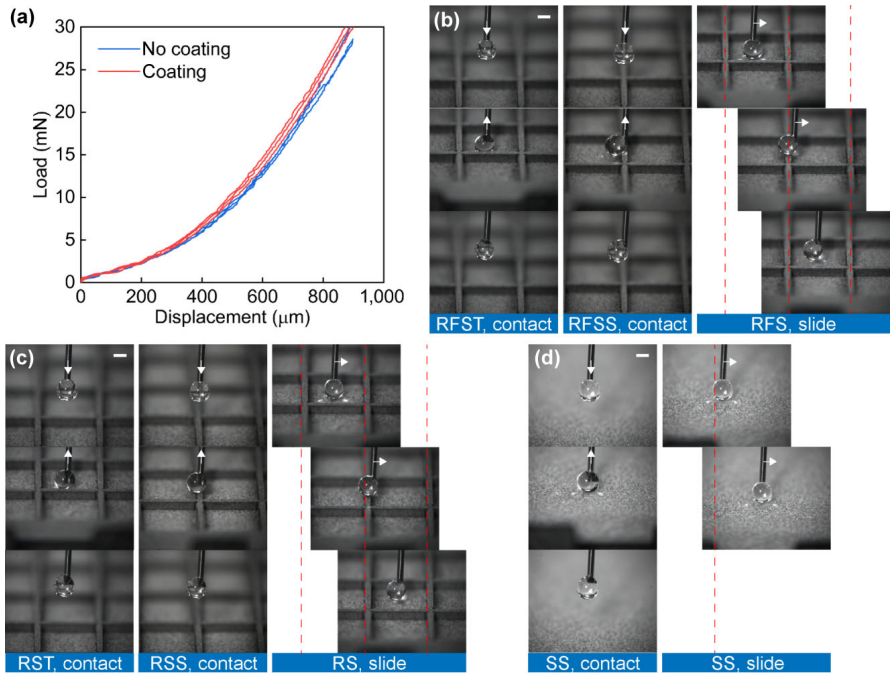


**Fig. 3** Static water repellency. (a) Mechanics of flexible trampolines on the RFS by measuring the load–displacement relationship. (b) Water droplets contacting and sliding over the RFS. (c) Water droplets contacting and sliding over the RS. (d) Water droplets contacting and sliding over the SS. Scale bar: 1 mm.

RFST during the droplet–surface contacting or sliding stage, indicating the low pressure generated by the static water droplets in relation to the mechanical properties of flexible trampolines.

Moreover, we quantified the values of contact angle by dripping water droplets from a micropipette with a low velocity because a hanging droplet cannot be trapped by the surfaces. The quantification was only performed on the trampolines of the RFS and RS. The RFST and RST exhibited the contact angles of 95.79°±0.57° and 98.60°±0.40°, respectively, which were smaller than the value of 159.57°±0.37° for the SS, appearing to imply weak water repellency. In fact, the contact angle is a macroscopic index based on a specified baseline so that the RFST and RST will characterize a reduced value due to the view blocked by the walls of the stripes.

### 3.3 Kinetic water repellency

We conducted impacting tests to gauge kinetic water repellency (including impalement resistance and contact time) of the fabricated surfaces against impinging droplets with different velocities. We selected the center as the impacting position for six trampolines and four stripes, as depicted in Fig. 4(a).

With regard to impalement resistance, Figure 4(b) shows the outcomes of impacting events along with an increased Weber number (*We*). Here, $We = D_0\rho V_0^2/\sigma$ is a nondimensionalized index to quantify the ratio between inertial and capillary forces; $\rho$ and $\sigma$ are the droplet density and tension, respectively; and $D_0$ and $V_0$ are the droplet diameter and velocity before the contacting instant, respectively. As per to the definition of the Wenzel and the Cassie–Baxter wetting states [28], we defined the outcomes of impacting events as follows. For the rebounding (REB), an impinging droplet spreads, retracts, and eventually bounces off the surface in its entirety (i in Fig. 4(b)). The REB can exhibit another three extensions, including REBUD (ii in Fig. 4(b)), REBLR (iii in Fig. 4(b)), and REBS (iv in Fig. 4(b)). Here, UD stands for the up–down segmentation; LR stands for the left–right segmentation; and S stands for the splashing behavior. Of note, in comparison to the REBUD occurring during the REB phase, the REBLR is a splitting behavior due to the asymmetric retraction [7, 8, 10–12], which has been adopted as a key indication for contact time reduction and will be verified later. Splashing is the behavior

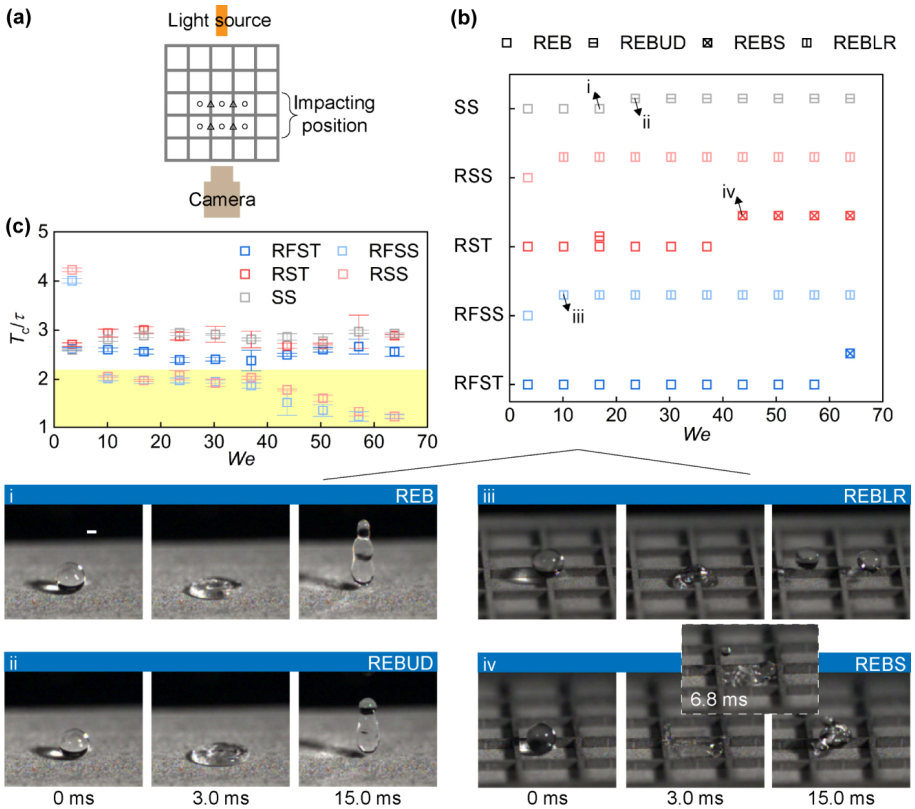


**Fig. 4** Kinetic water repellency. (a) Impacting position. (b) Outcomes of water droplets impacting the fabricated surfaces as a function of *We*, together with exemplary snapshots to visualize different impacting outcomes over time. (c) Dimensionless contact time ($T_c/\tau$) as a function of *We*, together with the theoretical inertia-capillarity limit of $T_c/\tau = 2.2$. Scale bar: 1 mm.

occurring during the spreading or retracting phase with small ejecting satellites due to the interaction of unstable liquid–gas interfaces at impact [29].

For the SS, the droplet exhibited the REB behavior and then transformed into the REBUD behavior as *We* increased, indicating good impalement resistance against droplet intrusion. The RST also manifested as good impalement resistance in relation to impacting droplets. However, after the REB–REBUD transformation, the REBUD behavior suddenly disappeared at $We \approx 23.5$ and was inherited by the REB behavior again, which can be ascribed to the fact that the droplet spread large enough to touch the walls of the stripes. Then, the REB behavior eventually changed to the REBS behavior when *We* raised up to ~43.7, and the amount or the size of ejecting satellites increased when *We* continued to increase. In comparison to the SS and RST, the RFST did not present the REBUD response, which can be ascribed to the reduced impacting load arising from structural oscillation. The reduced impacting load also delayed the occurrence of the REBS to ~63.8. The RFSS and RSS exhibited the synchronous occurrence of REB–REBLR transformation at $We \approx 10.1$ due to the same stripe design.

With a view to explore how our design can affect contact time, Figure 4(c) shows the contact time ($T_c$) along with an increased *We*, where $T_c$ is non-dimensionalized by a timescale ($\tau = 0.125\,\rho D_0^3/\sigma^{0.5}$) [6]. The yellow shade denotes the theoretical limit of 2.2 by balancing inertial and capillary forces [6]. The RST exhibited a nearly overlapped contact time in comparison to the SS. The RFST exhibited an obvious reduction in relation to the RST and SS, confirming the flexibility-based structural oscillation, in consistent with the findings in previous studies about flexible water-repelling surfaces [13–17]. However, the contact time did not break through the theoretical limit due to the absence of pancake-like bouncing [30]. As the view was blocked by the walls of the stripes, it is difficult to directly capture the trampoline displacements. Thanks to momentum conservation theory, the impacting load can be theoretically

estimated by $0.25\pi\rho D_0^2 V_0^2$ that denotes an impacting pressure $\rho V_0^2$ over an area $0.25\pi D_0^2$ [31]. Based on the estimated impacting load, the trampoline displacement can be evaluated referring to the load–displacement relationship established in Fig. 3(a). When the impacting load ranged from 0.47 to 8.93 mN, and when *We* changed from ~3.4 to ~63.8, the maximum trampoline displacement was evaluated around 600 μm. As depicted in Fig. 4(c), the deviation of contact time between the RFST and the RST (or SS) increased as *We* increased, but was interrupted at the maximum value of 20.1% at *We* ≈ 23.5, which can be ascribed to the touch between the spreading droplet and the stripe walls, in consistent with the REBUD disappearance for the RST at *We* ≈ 23.5 in Fig. 4(b). Accordingly, we can boldly assume that the trampoline displacement would decrease owing to the droplet–wall touch. When a droplet impacted the convex stripes (RFSS and RSS in Fig. 4(c)), the rigidity-based asymmetric redistribution principle was triggered to remarkably reduce the contact time, breaking through the theoretical limit in line with previous works about rigid water-repelling surfaces [7–12, 17]. It can be concluded that our RFS surface has combined the asymmetric redistribution and structural oscillation principles for water-repelling, overcoming the strict requirement on impacting positioning.

### 3.4 Abrasion resistance

We conducted rubbing tests to gauge the abrasion resistance of the fabricated surfaces. In the most recent related work [26], superhydrophobic surfaces made of silicon, glass, ceramic, and aluminum were rubbed with a 1 mm × 5 mm polypropylene surface at a normal load of 3 N and a velocity of 5 mm·s$^{-1}$, retaining water repellency after 1,000 cycles. In our test, a 15-mm triangular oilstone with an angle of 85° was declined to approach a line contact with the surfaces at a normal load of 3 N, and was then slid over the fabricated surfaces at a velocity of 1 mm·s$^{-1}$ for 1,000 cycles (Fig. 5(a)). Of note, first, we have selected a line-contact mode rather than a surface-contact mode because the surface-contact mode requires strict experimental conditions (e.g., parallelism of the rubbing pair, flatness of each surface, etc.) than the line-contact one. The normal load of 3 N generated a

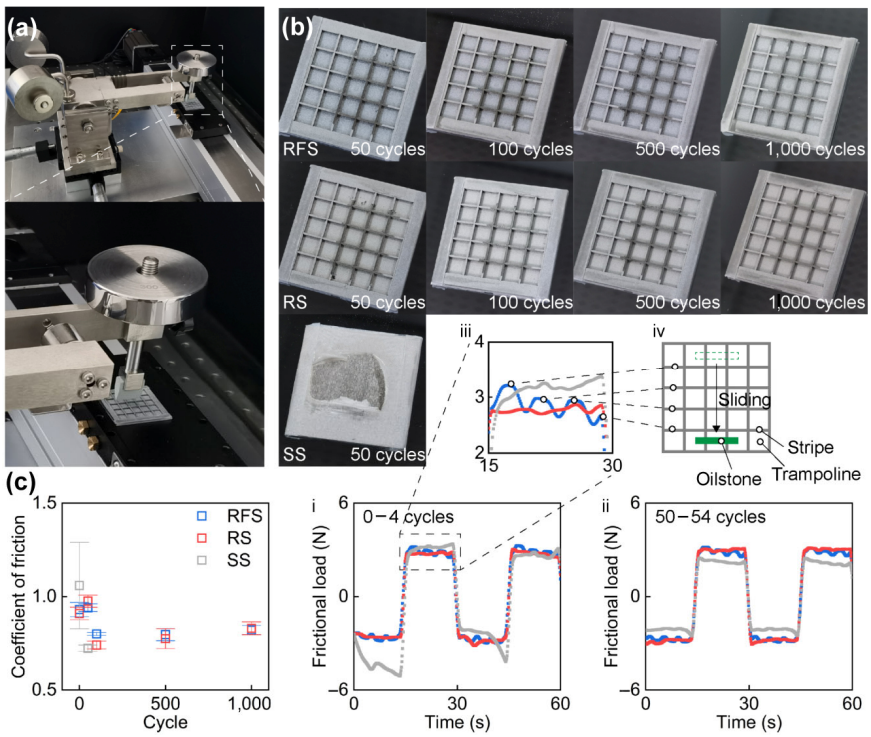


**Fig. 5** Abrasion resistance. (a) Tribological test rig. (b) Images of the fabricated surfaces after 50, 100, 500, and 1,000 abrasion cycles. (c) Coefficient of friction as a function of abrasion cycle, together with two examples (0–4 cycles and 50–54 cycles) to demonstrate frictional behaviors.

line pressure of 0.2 N·mm$^{-1}$ in our study but an area pressure of 0.6 N·mm$^{-2}$ in the reference. Second, as per to the standard suggestion on abradant materials (i.e., textile, rubber, and sandpaper) [21], we have substituted polypropylene with oilstone. Also, we have selected steel for water-repelling surfaces rather than silicon, glass, or ceramic because the steel is widely used in machinery equipment. Third, we have changed the sliding velocity from 5 to 1 mm·s$^{-1}$. In previous studies about water-repelling surfaces, researchers mainly linked sliding conditions (e.g., applied load, sliding distance, etc.) to surface change (e.g., morphological change, chemical change, etc.). This can be grouped into the material removal or transfer, which is usually termed as wear in the research field of tribology. In this study, we wish to introduce more tribological factors, such as coefficient of friction, into water-repelling surface investigation to discuss the interaction of the rubbing pair (termed as friction in the research field of tribology), helping the reveal of abrasion mechanism. A sliding velocity of 5 mm·s$^{-1}$ is extremely fast in relation to the structural size of the fabricated surfaces (e.g., side length of trampolines is only 4,560 μm), and will miss useful information.

Figure 5(b) shows the fabricated surfaces after 50, 100, 500, and 1,000 abrasion cycles. As the PVC film was destroyed after 50 cycles, we stopped the abrasion test for the SS. For the RFS and RS, the trampolines were protected because the normal pressure and horizontal shear were undertaken by the convex stripes. However, the low-surface-energy chemical particles (in white) on the stripes were removed. Moreover, small-size debris (in black) were generated, indicating the material wear for the stripes made of steel.

Figure 5(c) shows the coefficients of friction during the 1st, 50th, 100th, 500th, and 1,000th cycle abrasion, providing the cases at the beginning of abrasion test (i in Fig. 5(c)) and after 50 abrasion cycles (ii in Fig. 5(c)) as examples to demonstrate frictional behaviors. As the abrasion test started (i in Fig. 5(c)), the interaction of the sliding pair produced a horizontal shear (also termed as frictional load) that varied with time. And the sign symbol instantaneously alternated every 15 s (equaling to the cycle period), confirming a reciprocating motion. As depicted in the inset (iii in Fig. 5(c)), the frictional load for the RFS and RS had a fluctuation with time. As illustrated by the schematic (iv in Fig. 5(c)), each extreme point within the fluctuation of frictional loads occurred when the oilstone slid over a stripe. Of note, the fluctuant amplitude for the RFS was larger than that for the RS, indicating a larger structural deformation on the stripes of the RFS under a horizontal shear due to the different design for the bottom part (Fig. 1(a) vs. Fig. 2(a)). Also noteworthy is an unsymmetrical frictional load for the SS in the alternated sliding directions (i in Fig. 5(c)), which can be ascribed to the partial breakage of the PVC film. This asymmetry faded away (ii in Fig. 5(c)) as the abrasion cycle increased to enlarge the film breakage. Returning back to the coefficient of friction, it increased initially but then decreased when the cycle number increased from 0 to 100, relating to the running-in stage to construct the optimized sliding state. When the cycle number continued to raise up, the coefficient of friction kept a nearly constant value, entering the stable stage which usually implies stable tribological performance.

We further investigate the water repellency of the fabricated surfaces after the abrasion test. With regard to static water repellency, the worn surfaces were controlled to contact and slide over hanging water droplets. As soon as the SS contacted the droplet (Fig. 6(a)), the droplet was rapidly trapped by the surface, indicating the hydrophilicity of the SS due to the exposure of the steel substrate after abrasion. For the RFS and RS, the same phenomenon can be observed when the droplet contacted or slid over the top side of the stripes. However, the droplet beaded up on the trampolines and was eventually trapped by the needle, indicating the fact that the convex rigid stripes sacrificed themselves under abrasion to protect the water-repelling trampolines.

With regard to kinetic water repellency, Fig. 6(b) shows the outcomes of impacting events at $We \approx 23.5$ to gauge the impalement resistance. For the SS, the droplet changed from the REBUD behavior to the pinning (PIN) behavior after abrasion. The droplet did not bounce off the surface after the retraction but pinned onto the surface (i in Fig. 6(b)), indicating the failure of impalement resistance. Gratifyingly, the RFS and RS retained the initial outcomes even after 1,000 abrasion cycles, confirming great impalement resistance against impacting droplets. Of note, as the low-surface-energy chemical coating on the top side

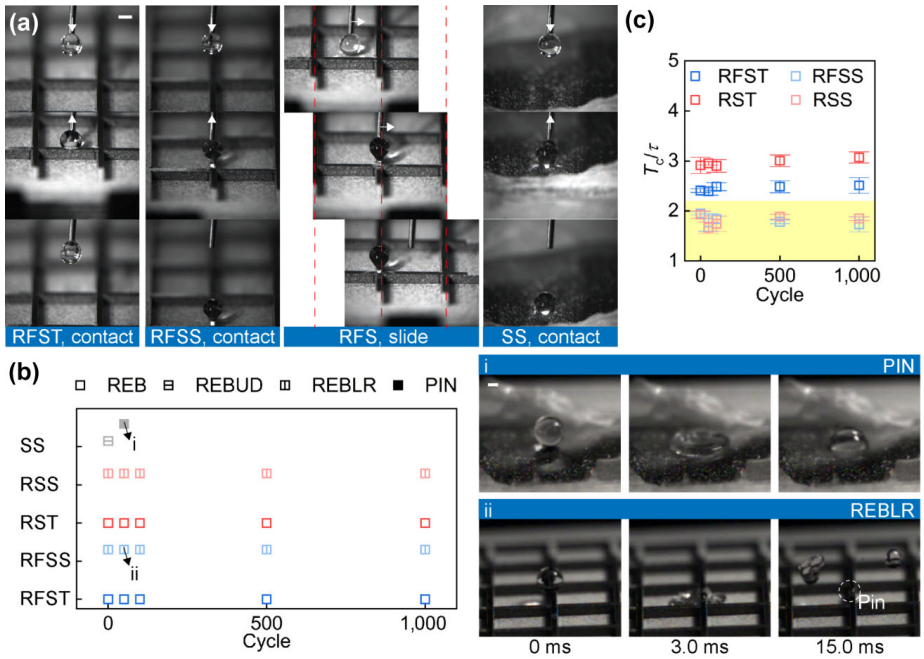


**Fig. 6** Kinetic water repellency after abrasion. (a) Contact angle and adhesion of water droplets contacting and sliding over the fabricated surfaces. (b) Outcomes of water droplets impacting the fabricated surfaces as a function of abrasion cycle, together with exemplary snapshots to visualize different impacting outcomes over time. (c) $T_c/\tau$ as a function of abrasion cycle, together with the theoretical inertia-capillarity limit of $T_c/\tau = 2.2$. Scale bar: 1 mm.

of the stripes was removed by abrasion, part of the droplet pinned onto the top side of the stripes (dash circle in ii of Fig. 6(b)) when the droplet split into the left and right satellites. Moreover, the RFS and RS kept the contact time along with the abrasion test (Fig. 6(c)).

## 4 Conclusions

For water-repelling and abrasion-resisting, we designed the artificial surface as a matrix of concave flexible trampolines barred by convex rigid stripes, yielding an RFS. In the realm of water-repelling, such a design is of great significance because it tunes droplet bouncing through a synergistic effect, i.e., droplet–surface contact time is envisioned to be reduced by asymmetric redistribution and structural oscillation when the impact occurs on rigid stripes and flexible trampolines, thus resolving the strict requirement on impacting positioning. Also, in the realm of abrasion-resisting, the convex rigid stripes can act as armors to undertake normal pressure and horizontal shear so as to protect the concave flexible trampolines that are water-repelling but mechanically fragile. The surface is shown to achieve a 20.1% contact time reduction via the structural oscillation of flexible trampolines, and even to break through the theoretical inertial-capillary limit via the asymmetric redistribution induced by rigid stripes. Also, the surface is shown to retain the above water-repelling after 1,000 abrasion cycles against oilstones under the normal load as high as 0.2 N·mm$^{-1}$. We believe this study to be the very first demonstration of RFSs for synchronous waterproof and wearproof, approaching real-world applications of liquid-repelling.

## Acknowledgements

This work was supported by the National Natural Science Foundation of China (12002202), Young Elite Scientist Sponsorship Program by the China Association for Science and Technology (YESS20200403), and State Key Laboratory of Mechanical System and Vibration (MSVZD202104).

## References

[1] Schutzius T M, Jung S, Maitra T, Graeber G, Köhme M, Poulikakos D. Spontaneous droplet trampolining on rigid superhydrophobic surfaces. *Nature* **527**(7576): 82–85 (2015)

[2] Vasileiou T, Schutzius T M, Poulikakos D. Imparting icephobicity with substrate flexibility. *Langmuir* **33**(27): 6708–6718 (2017)

[3] Xu W H, Zheng H X, Liu Y, Zhou X F, Zhang C, Song Y X, Deng X, Leung M, Yang Z B, Xu R X, et al. A droplet-based electricity generator with high instantaneous power density. *Nature* **578**(7795): 392–396 (2020)

[4] Sun Q Q, Wang D H, Li Y N, Zhang J H, Ye S J, Cui J X, Chen L Q, Wang Z K, Butt H J, Vollmer D, et al. Surface charge printing for programmed droplet transport. *Nat Mater* **18**(9): 936–941 (2019)

[5] Li L Y, Zhu J F, Zeng Z X, Liu E Y, Xue Q J. Effect of surface roughness on the angular acceleration for a droplet on a super-hydrophobic surface. *Friction* **9**(5): 1012–1024 (2021)

[6] Richard D, Clanet C, Quéré D. Contact time of a bouncing drop. *Nature* **417**(6891): 811 (2002)

[7] Bird J C, Dhiman R, Kwon H M, Varanasi K K. Reducing the contact time of a bouncing drop. *Nature* **503**(7476): 385–388 (2013)

[8] Gauthier A, Symon S, Clanet C, Quéré D. Water impacting on superhydrophobic macrotextures. *Nat Commun* **6**: 8001 (2015)

[9] Liu Y H, Andrew M, Li J, Yeomans J M, Wang Z K. Symmetry breaking in drop bouncing on curved surfaces. *Nat Commun* **6**: 10034 (2015)

[10] Shen Y, Tao J, Tao H, Chen S, Pan L, Wang T. Approaching the theoretical contact time of a bouncing droplet on the rational macrostructured superhydrophobic surfaces. *Appl Phys Lett* **107**(11): 111604 (2015)

[11] Song M R, Liu Z H, Ma Y J, Dong Z C, Wang Y L, Jiang L. Reducing the contact time using macro anisotropic superhydrophobic surfaces—Effect of parallel wire spacing on the drop impact. *NPG Asia Mater* **9**(8): e415 (2017)

[12] Hu S T, Reddyhoff T, Puhan D, Vladescu S C, Shi X, Dini D, Peng Z K. Droplet manipulation of hierarchical steel surfaces using femtosecond laser fabrication. *Appl Surf Sci* **521**: 146474 (2020)

[13] Vasileiou T, Gerber J, Prautzsch J, Schutzius T M, Poulikakos D. Superhydrophobicity enhancement through substrate flexibility. *PNAS* **113**(47): 13307–13312 (2016)

[14] Weisensee P B, Tian J J, Miljkovic N, King W P. Water droplet impact on elastic superhydrophobic surfaces. *Sci Rep* **6**: 30328 (2016)

[15] Kim J H, Rothstein J P, Shang J K. Dynamics of a flexible superhydrophobic surface during a drop impact. *Phys Fluids* **30**(7): 072102 (2018)

[16] Chantelot P, Coux M, Clanet C, Quéré D. Drop trampoline. *Europhys Lett* **124**(2): 24003 (2018)

[17] Hu S T, Cao X B, Reddyhoff T, Shi X, Peng Z K, deMello A J, Dini D. Flexibility-patterned liquid-repelling surfaces. *ACS Appl Mater Interfaces* **13**(24): 29092–29100 (2021)

[18] Milionis A, Loth E, Bayer I S. Recent advances in the mechanical durability of superhydrophobic materials. *Adv Colloid Interface Sci* **229**: 57–79 (2016)

[19] Jin H, Tian X L, Ikkala O, Ras R H A. Preservation of superhydrophobic and superoleophobic properties upon wear damage. *ACS Appl Mater Interfaces* **5**(3): 485–488 (2013)

[20] Hensel R, Finn A, Helbig R, Braun H G, Neinhuis C, Fischer W J, Werner C. Biologically inspired omniphobic surfaces by reverse imprint lithography. *Adv Mater* **26**(13): 2029–2033 (2014)

[21] Tian X L, Verho T, Ras R H A. Moving superhydrophobic surfaces toward real-world applications. *Science* **352**(6282): 142–143 (2016)

[22] Xiu Y H, Liu Y, Hess D W, Wong C P. Mechanically robust superhydrophobicity on hierarchically structured Si surfaces. *Nanotechnology* **21**(15): 155705 (2010)

[23] Verho T, Bower C, Andrew P, Franssila S, Ikkala O, Ras R H A. Mechanically durable superhydrophobic surfaces. *Adv Mater* **23**(5): 673–678 (2011)

[24] Kondrashov V, Rühe J. Microcones and nanograss: Toward mechanically robust superhydrophobic surfaces. *Langmuir* **30**(15): 4342–4350 (2014)

[25] Hoshian S, Jokinen V, Somerkivi V, Lokanathan A R, Franssila S. Robust superhydrophobic silicon without a low surface-energy hydrophobic coating. *ACS Appl Mater Interfaces* **7**(1): 941–949 (2015)

[26] Wang D H, Sun Q Q, Hokkanen M J, Zhang C L, Lin F Y, Liu Q, Zhu S P, Zhou T F, Chang Q, He B, et al. Design of robust superhydrophobic surfaces. *Nature* **582**(7810): 55–59 (2020)

[27] Wen J, Reddyhoff T, Hu S T, Puhan D, Dini D. Exploiting air cushion effects to optimise a superhydrophobic/hydrophilic patterned liquid ring sealed air bearing. *Tribol Int* **144**: 106129 (2020)

[28] Hu S T, Reddyhoff T, Puhan D, Vladescu S C, Huang W F, Shi X, Dini D, Peng Z K. Bi-Gaussian stratified wetting model on rough surfaces. *Langmuir* **35**(17): 5967–5974 (2019)

[29] Tsai P, Hendrix M H W, Dijkstra R R M, Shui L L, Lohse D. Microscopic structure influencing macroscopic splash at high Weber number. *Soft Matter* **7**(24): 11325–11333 (2011)

[30] Liu Y H, Moevius L, Xu X P, Qian T Z, Yeomans J M, Wang Z K. Pancake bouncing on superhydrophobic surfaces. *Nat Phys* **10**(7): 515–519 (2014)

[31] Soto D, de Larivière A B, Boutillon X, Clanet C, Quéré D. The force of impacting rain. *Soft Matter* **10**(27): 4929–4934 (2014)

**Songtao HU.** He received his Ph.D. degree from Tsinghua University, China, in 2017. He is now an associate professor at Shanghai Jiao Tong University, China. His research interests include intelligent sensors and actuators, operation and maintenance, and surfaces.

**Weifeng HUANG.** He received his Ph.D. degree from Tsinghua University, China, in 2006. He is now an associate researcher at Tsinghua University, China. His research interests include advanced fluid sealing and microscale flow.

**Jinbang LI.** He received his Ph.D. degree from Harbin Institute of Technology, China, in 2016. He is now an associate professor at Ningbo University, China. His research interests include tribology and piezoelectric precision drive system.

**Tom REDDYHOFF.** He received his Ph.D. degree from the University of Sheffield, UK, in 2006. He is now a reader at Imperial College London, UK. His research interests include experimental techniques and numerical modelling on fluid lubrication.

**Xiaobao CAO.** He received his Ph.D. degree from ETH Zurich, Switzerland, in 2019. He is now a postdoctoral research fellow at ETH Zurich, Switzerland. His research interests include microfluidics and biological analysis.

**Xi SHI.** He received his Ph.D. degree from the University of Illinois at Urbana-Champaign, USA, in 2005. He is now a professor at Shanghai Jiao Tong University, China. His research interests include industrial tribology, industrial big data, and intelligent operation and maintenance.

**Zhike PENG.** He received his Ph.D. degree from Tsinghua University, China, in 2002. He is now a professor at Shanghai Jiao Tong University, China, and Ningxia University, China. His research interests include signal analysis and intelligent operation and maintenance.

**Andrew DEMELLO.** He received his Ph.D. degree from Imperial College London, UK, in 1995. He is now a professor at ETH Zurich, Switzerland. His research interests include microfluidics and nanoscale science.

**Daniele DINI.** He received his Ph.D. degree from the University of Oxford, UK, in 2004. He is now a professor at Imperial College London, UK. His research interests include tribology, applied mechanics, and materials.